MATHEMATICA APPLICANDA
Vol. 48(1) 2020, p. 25–48
doi: 10.14708/ma.v48i1.6507

Zofia Wróblewska (Wrocław)

Approximate solutions and numerical analysis of a spring-mass running model

Abstract The paper refers to the classic spring-mass model of running, which was created on the basis of an inverted elastic pendulum. A new approximate solution of the boundary value problem relayed to the governing system based on two nonlinear ordinary differential equations is introduced, which we get in this model in a natural way. We give theoretical support by deriving asymptotic behaviour of obtained approximations. Simulations show that new solutions turn out very well. Our results are illustrated with some practical examples.

2010 Mathematics Subject Classification: Primary: 34E05; Secondary: 34B15.

Key words and phrases: spring-mass model, running, elastic pendulum, boundary value problem, approximation solution, shooting method.

1. Introduction Running is the most intuitive way used by some terrestrial animals to move fast. Running has accompanied a man as a primal form of movement from the very beginning. It seems that there is nothing unusual about it. Nevertheless, this form of movement requires accurate and complex cooperation of systems such as muscular, motor and neural [10]. On the other hand, one has to agree with the fact that running is characterized by simplicity and is seen as the most natural sport that exists [2]. Therefore, it is a basis of a various sport disciplines. In sport science it is quite common to analyze and attempt to describe particular movements specific to a considered discipline. However, running is one of the most important motor skills. Its improvement can implicate a huge progression in overall results in a given discipline. That is why the running analysis forms the core of this paper. Better understanding of human performance during races provides better insights into improved training methods (cf. [3], [9], [33], etc).

The difference between gait and running can be defined by an aerial phase that lacks contact with the ground and which is common only for running. All feet are in the air at some point in the run cycle, whereas in the gait there is always at least one foot placed on the ground. Furthermore, running is not just walking at a higher speed, and there is a notable transition of one mode of motion to the other. The analysis of the run should start with an observation of how running bipedal terrestrial animals move.

The astonishing elegance and efficiency with which animals' legs traverse natural terrain outclasses any present day man-made competitor. Beyond sheer fascination, such a technological superiority heavily attracts the interest of many scientists. Over the decades, the legged locomotion has been under close investigations. It combines biology, mathematics and engineering into one successful endeavour and is typical of various animals. Aristotle [27] was the first to explore the topic, then, the seventeenth century Italian mathematician and physiologist Giovanni Borelli [19] investigated the subject and gave the first biomechanical treatment. Modern surveys relates to the scientific accounts of locomotion can be found in [17].

It seems, however, that despite intensive research activities in fields as diverse as biomechanics, robotics and medicine, the overwhelming complexity of biological systems can deny a comprehensive understanding of all functional details of the leg movement apparatus. Using some simplifications, without claiming to capture the whole system, any obtained models may well be suited to succeed in identifying some underlying principles of pedal locomotion. In running, as a fundamental way of rapid leg locomotion, a bouncing gait is used. Several recent findings suggest an analogy to hopping by a simple spring mass system. The skeletal system is considered in mechanical terms and it is assumed that it behaves simply like a point mass bouncing passively on a massless spring. In this paper the conceptual spring-mass model will be revisited. For a thorough analysis we refer to [4] and [20]. It will be based on an inverted elastic pendulum for each leg.

On the other hand, some earlier attempts to describe gait using a similar construction utilizing an inverted pendulum (see [22]) led to a proliferation of models, methods and interesting concepts that helped to create walking robots (see [7]). The subsequent spring-mass model generalizations include dampers, additional legs and segments (cf. [14], [21], [30], [31] and [32]). A completely different approach to construct the model of legged locomotion was proposed in [18]. The authors of [18] presented several algorithms using the learning processes. In consequence, not only biomechanical studies investigating running, but also fast legged robots driven by model-based control algorithms are an important part of the deliberations under consideration.

In this paper we introduce new approximate solutions of a boundary value problem concerning the governing system related to the two nonlinear ordinary differential equations, which we get in a natural way in the classic spring-mass model of running. It requires us to choose the stiffness in order to ensure that the spring returns to its initial, equilibrium position after a complete step. An asymptotic analysis of the main equations with the use of the Poincaré - Lindstedt series was carried out in [28]. The solution of the problem is based on the perturbative expansion related to the significant spring stiffness. In addition, the authors of [28] used the obtained asymptotic estimates to prove that there is a unique solution to the previously mentioned boundary value problem. Moreover, they provide an approximation to the sought stiffness.

Mathematical modelling is an important part of biomechanics. When modeling such a complex object as the human body, it is good to start with a simple case. That is why at the beginning, hopping in place with a vertical velocity was described. After getting some intuition and adding horizontal velocity, a target model of hopping forward was considered. Next, some attempts have been made to model running using the best possible simplifications.

This paper is organized as follows. The spring-mass model for running is introduced in Section 2. Section 3 contains an analysis based on the approximate solution to the governing equations. Numerical methods can be found in Section 4. Finally, conclusions and an illustration on real data examples of how the solution works are given in Sections 6 and 5, respectively.

2. The spring-mass model In this section we present a mathematical model for terrestrial running, based on a leg with properties of a simple spring. Such a spring-mass system for hopping forward is described, among others, in the papers [4], [16] and [20].

Under the assumption that only gravitational force (F_g) depends on body mass (m) and spring force (F_s) play a role, Newton's second law of motion and Hooke's law of elasticity lead to the following physical equation during the contact phase:

$$F = F_g + F_s,$$

where $F = ma$, $F_g = -mg$, $F_s = k\Delta l$ and also k denotes the spring stiffness while Δl stands for the change in the leg length.

In what follows we will provide a mathematical description of that model.

2.1. Model derivation The model for hopping forward (for example, like a kangaroo) contains besides the kinematic variables (y, v_y, a_y, F_y) also (x, v_x, a_x, F_x). Quantities such as speed and force are decomposed in the x- and y-directions. The planar inverted spring-mass model for bouncing gaits such as hopping and running is schematised in Figure 1 (see below).

Hopping forward introduces the leg length as an additional parameter in the differential equations of the spring-mass model. Contact time not only depends on the spring stiffness and the vertical landing velocity, but also on the human's speed and leg length.

Furthermore, we introduce two new angle conditions not found in the simple one dimensional spring mass model of upward hopping. Namely, the angle between the leg and ground at contact α (the leg angle of attack), and the angle of velocity when contact is lost β (the angle of taking-off velocity). These angles are most easily defined when we select the stance point as the origin of the coordinate system during the contact phase, with the positive x-axis in the direction of motion and the positive y-axis in the upward direction. And in addition when we assume that the stance leg lands at time $t = 0$: $\tan(\alpha) = -x_0/y_0$ and $\tan\beta = v_y/v_x$ (see Figure 1), where v_x is the horizontal landing and take-off speed, $-v_y$ and v_y are the vertical landing and take-off

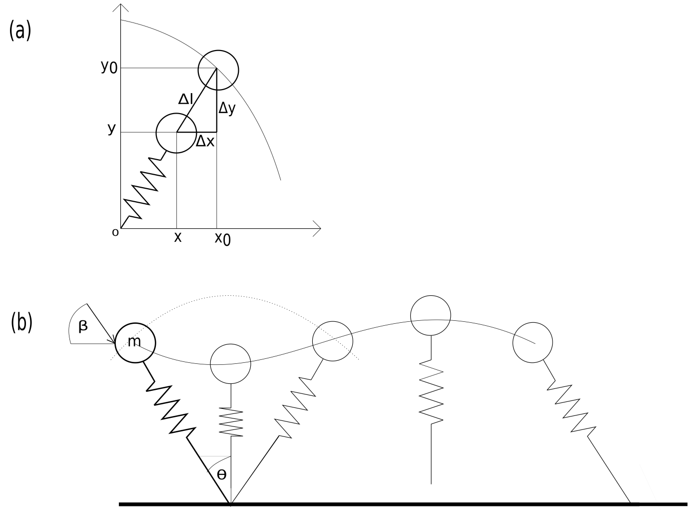

Figure 1: The planar model, where velocity and displacement become vector quantities. (a) The compression of the spring (Δl) can be represented by a horizontal (Δx) and vertical (Δy) components. (b) Only stationary movements were selected from all simulated hops. Symmetrical take off and landing velocities (v), β - angle of landing velocity, $\theta = -\alpha$ - angle of attack of the spring were assumed.

speed. Note that leg angle of attack and the angle of take-off velocity are not necessarily equal ($\alpha \neq \beta$).

(A) During **the contact phase** the planar movement from Newton's second law of motion can be described by two nonlinear differential equations

$$\begin{cases} \ddot{x} = \omega^2 \left(l_0 - \sqrt{x^2 + y^2} \right) \sin\theta, \\ \ddot{y} = \omega^2 \left(l_0 - \sqrt{x^2 + y^2} \right) \cos\theta - g, \end{cases} \tag{1}$$

where x is horizontal deflection, y - vertical deflection, g - gravitational acceleration, $\omega = \sqrt{\frac{k}{m}}$ - natural frequency of a spring-mass system, k - spring stiffness, m - mass and $l_0 = \sqrt{{x_0}^2 + {y_0}^2}$ - the starting and ending length of the spring. The initial conditions (ICs), in this case, are

$$\begin{array}{ll} x(0) = -l_0 \sin\alpha, & y(0) = l_0 \cos\alpha, \\ \dot{x}(0) = v\cos\beta = v_x, & \dot{y}(0) = -v\sin\beta = -v_y, \end{array} \tag{2}$$

where v_x is horizontal take-off speed and v_y - vertical take-off speed. In addition, angles α, β and deflections $x_0 = x(0)$, $y_0 = y(0)$ are defined in Figure 1.

(B) During **the aerial phase** ($F_s = 0$) the equations of motion are

$$\begin{array}{lll} \ddot{x} = 0, & \dot{x}(0) = v_x, & x(0) = l_0 \sin\alpha, \\ \ddot{y} = -g, & \dot{y}(0) = v_y, & y(0) = l_0 \cos\alpha. \end{array} \tag{3}$$

Thus, the solutions of (3) are as follows

$$x = l_0 \sin\alpha + v_x t \ \text{ and } \ y = l_0 \cos\alpha + v_y t - \frac{gt^2}{2}. \tag{4}$$

Therefore, from (4) and because of $y(t_a) = l_0 \cos\alpha$, where t_a is aerial time, we get

$$v_y = \frac{gt_a}{2} \ \text{ and } \ t_a = \frac{2v_y}{g}. \tag{5}$$

2.2. Nondimensionalization and problem statement In this section we will analyze nonlinear equations (1), which describe running during the contact phase with initial conditions (2).

In order to transform the equations of motion (1) and initial conditions (2) into a tractable dimensionless form we introduce the following dimensionless variables:

$$X = \tfrac{x}{l_0}, \quad Y = \tfrac{y}{l_0}, \quad L = \tfrac{\sqrt{x^2+y^2}}{l_0} = \sqrt{X^2+Y^2} \quad \text{and} \quad T = t\sqrt{\tfrac{g}{l_0}}.$$

For ease of computation we have normalised lengths with respect to l_0, and we have multiplied the time by the group $(g/l_0)^{1/2}$ to make time dimensionless. We note that this group happens to be the (small-amplitude) frequency of a pendulum made by hanging the mass from the (unstretched) leg. It is easy to see that

$$\begin{array}{ll} \dot{X} = \dfrac{\partial X}{\partial T} = \dfrac{\dot{x}/l_0}{(g/l_0)^{1/2}} = \dfrac{\dot{x}}{(gl_0)^{1/2}} & \text{and} \quad \dot{Y} = \dfrac{\partial Y}{\partial T} = \dfrac{\dot{y}/l_0}{(g/l_0)^{1/2}} = \dfrac{\dot{y}}{(gl_0)^{1/2}}, \\ \ddot{X} = \dfrac{\partial^2 X}{\partial T^2} = \dfrac{\ddot{x}/l_0}{g/l_0} = \dfrac{\ddot{x}}{g} & \text{and} \quad \ddot{Y} = \dfrac{\partial^2 Y}{\partial T^2} = \dfrac{\ddot{y}/l_0}{g/l_0} = \dfrac{\ddot{y}}{g}. \end{array}$$

Below, the differential equations (1) will be analysed in the following dimensionless form (see also Appendix B in [20])

$$\begin{cases} \ddot{X} = (\ddot{x}/g) = (l_0\omega^2/g)(1-L)\sin\theta = K(1-L)\sin\theta, \\ \ddot{Y} = (\ddot{y}/g) = (l_0\omega^2/g)(1-L)\cos\theta - 1 = K(1-L)\cos\theta - 1, \end{cases} \tag{6}$$

where $K = l_0\omega^2/g = kl_0/mg$ - dimensionless leg stiffness. We note that the product kl_0 is the greatest force that can be developed by the leg-spring, i.e. the force exerted by the fully compressed spring. Therefore, a ratio of $kl_0/mg < 1$ means that the force developed by the spring cannot overcome the weight. We can also consider the ratio $l_0\omega^2/g$ which is the square of the ratio of the natural frequency of the mass-spring system to the natural frequency of the leg as a pendulum.

As an interesting consequence of substituting the assumed normalization for length and time into the conditions on the initial (and final) velocities, we have that these velocities are divided by a reference velocity $(gl_0)^{1/2}$. This reference velocity has a simple meaning. An inverted pendulum of length l_0 swinging through the top of its arc would fly off the ground if the speed of its mass were greater than $(gl_0)^{1/2}$. In fluid mechanics, a velocity made dimensionless by the factor (acceleration of gravity $\times$ length)$^{1/2}$ is called the Froude number.

The initial conditions (*ICs*) given by (2), in this case, are reduced to the form

$$\begin{array}{ll} \theta(0) = -\alpha, & L(0) = 1, \\ \dot{X}(0) = v_x(gl_0)^{-\frac{1}{2}} = V_X, & \dot{Y}(0) = -v_y(gl_0)^{-\frac{1}{2}} = -V_Y, \end{array} \tag{7}$$

where V_X is the horizontal Froude number and V_Y - the vertical Froude number.

At the beginning of the rebound, the horizontal mass velocity $\dot{x}$ is v_x while the vertical velocity $\dot{y}$ is $-v_y$ (see (2)). Moreover, during the rebound, we assume that the angle of the leg with respect to the vertical axis begins at $-\alpha$ and ends $+\alpha$. In addition, the x-velocity begins and ends with the value v_x, and the y-velocity is reversed by the step, starting with the value $-v_y$ and ending with $+v_y$. Therefore, in addition to the initial conditions (7), we also assume the following final conditions (*FCs*) for equations (6)

$$\begin{array}{ll} \theta(T_c) = \alpha, & L(T_c) = 1, \\ \dot{X}(T_c) = V_X, & \dot{Y}(T_c) = V_Y, \end{array} \tag{8}$$

where T_c is dimensionless final contact time. The differential equations are given in the dimensionless form to make the results representative of animals of all body sizes.

It is both natural and beneficial to express the leading equations in polar coordinates. We know that

$$\sin\theta = \frac{x}{\sqrt{x^2+y^2}} \quad \text{and} \quad \cos\theta = \frac{y}{\sqrt{x^2+y^2}},$$

where θ is the polar angle and we have

$$X = L\sin\theta \quad \text{and} \quad Y = L\cos\theta. \tag{9}$$

Thus, the system of the first derivatives of X and Y is given by the formulas

$$\begin{aligned} \dot{X} &= \dot{L}\sin\theta + L\dot{\theta}\cos\theta, \\ \dot{Y} &= \dot{L}\cos\theta - L\dot{\theta}\sin\theta. \end{aligned} \tag{10}$$

Symbol	Description	Typical value
α	Angle of attack	$0.1 - 0.8$
V_X	Horizontal Froude number	$0.8 - 3.8$
V_Y	Vertical Froude number	$0.05 - 0.5$

Table 1: Typical values of all nondimensional parameters input for the simulations (cf. [11], [20] and also Sections 4 and 5).

Finally, we will present differential equations (6) in polar coordinates L and θ (see (9)). By inserting into the formulas (6) the second derivatives of X and Y, which are in forms

$$\begin{aligned} \ddot{X} &= \ddot{L}\sin\theta + 2\dot{L}\dot{\theta}\cos\theta - L\dot{\theta}^2\sin\theta + L\ddot{\theta}\cos\theta, \\ \ddot{Y} &= \ddot{L}\cos\theta - 2\dot{L}\dot{\theta}\sin\theta - L\dot{\theta}^2\cos\theta - L\ddot{\theta}\sin\theta, \end{aligned}$$

we get the following polar system

$$\begin{cases} L\ddot{\theta} + 2\dot{L}\dot{\theta} = \sin\theta, \\ \ddot{L} - L\dot{\theta}^2 = K(1-L) - \cos\theta, \end{cases} \tag{11}$$

where the only nondimensional parameter is the spring stiffness K.

To obtain the initial conditions, from (7) and (10), we have to solve the following system of equations

$$\begin{cases} \dot{\theta}(0)\cos\alpha & - & \dot{L}(0)\sin\alpha & = & V_X, \\ \dot{\theta}(0)\sin\alpha & + & \dot{L}(0)\cos\alpha & = & -V_Y. \end{cases}$$

Thus, the initial conditions (ICs) are represented by the formulas

$$\begin{aligned} &\theta(0) = -\alpha, \quad L(0) = 1, \\ &\dot{\theta}(0) = \theta_d, \quad\ \dot{L}(0) = -L_d, \end{aligned} \tag{12}$$

with

$$\theta_d = V_X\cos\alpha - V_Y\sin\alpha \quad \text{and} \quad L_d = V_X\sin\alpha + V_Y\cos\alpha \tag{13}$$

and using the dependence on the angle β (i.e. $\tan\beta = V_Y/V_X$) with

$$\theta_d = \frac{V_X\cos(\alpha+\beta)}{\cos\beta} \quad \text{and} \quad L_d = \frac{V_Y\sin(\alpha+\beta)}{\sin\beta}. \tag{14}$$

In Table 1 we have collected all nondimensional parameters appearing in the model. The data based on [11] is calculated for various animals. Notice that usually V_X is the order of unity, while V_Y and α are small.

As the forwardly hoping leg is modeled by the inverted elastic pendulum, a peculiar boundary value problem appears.

Problem *Let $(\theta(T,K), L(T,K))$ be the solution of the system (11) with (12). Find K^* and the smallest time $T^* > 0$ satisfying*

$$\theta(T^*, K^*) = \alpha, \quad L(T^*, K^*) = 1. \tag{15}$$

The spring stiffness K should be determined, so that during the first cycle the spring returns to the equilibrium length at the exact moment when the pendulum moves to the angle α. This means that the leg completes the full cycle before switching into the aerial phase (see Figure 1). Thus, the final conditions (*FCs*) are a symmetrical reflection of the initial ones (12) and have the form

$$\begin{aligned} \theta(T^*) &= \alpha, & L(T^*) &= 1, \\ \dot{\theta}(T^*) &= \theta_d, & \dot{L}(T^*) &= L_d, \end{aligned} \tag{16}$$

where θ_d and L_d are given by (13) or (14).

The nonlinear equations (11) with their initial and final conditions (12) and (16) constitute a two-point boundary value problem that can be solved using the shooting method (see Section 4).

3. Approximate solutions of nonlinear differential equations At the beginning of this section we consider approximating a solution to (11) with the boundary conditions (12) and (16). We derive an approximate solution in elementary functions assuming a small angle of attack α ($|\theta| \le \alpha$) and a small spring compression during the contact phase. Thus, the polar coordinates θ and L satisfy the following conditions:

$$\boxed{L \approx 1 \quad \text{and} \quad \begin{array}{lclcl} |\theta| \ll 1 & \Longrightarrow & \sin\theta \approx \theta & \text{and} & \cos\theta \approx 1, \\ |\dot{\theta}| \ll 1 & \Longrightarrow & \dot{L}\dot{\theta} \approx 0 & \text{and} & L\dot{\theta}^2 \approx 0. \end{array}}$$

The analysis shows that for spring compression of up to 20%, the angle of attack is smaller than 30° (i.e. $|\theta| \le 30°$) and the approximate solution describes the dynamics of the center of mass within a 1% tolerance of spring compression and 0.6° tolerance of angular motion compared to numerical calculations. For more comments and explanations we refer to [13], where a similar approximate solution, but for dimensional polar coordinates, was proposed by Geyer, Seyfarth and Blickhan. Thus, taking into account the above assumptions, our simplification of equations (11) is as follows

$$\begin{aligned} &\ddot{\theta} - \theta = 0, \\ &\ddot{L} + KL = K - 1. \end{aligned} \tag{17}$$

Equations (17) are already linear differential equations.

- The solution of the first equation of (17) is presented as follows

$$\widetilde{\theta}(T) = \theta_d \sinh T - \alpha \cosh T. \tag{18}$$

By application of the final condition $\widetilde{\theta}(T = \widetilde{T}_c) = \alpha$ (see (16)) we obtain

$$\coth(\widetilde{T}_c/2) = \frac{\theta_d}{\alpha}$$

and because the inverse hyperbolic cotangent is given by

$$\operatorname{arcoth} x = \frac{1}{2}\log\left(\frac{x+1}{x-1}\right)$$

we get the approximation of T_c with the formula

$$\widetilde{T}_c = \log\left(\frac{\theta_d+\alpha}{\theta_d-\alpha}\right), \tag{19}$$

where $\theta_d > \alpha$ or $\theta_d < -\alpha$.

- The solution of the second equation of (17) yields the approximation for L

$$\widetilde{L}(T) = 1 - \omega^{-1}L_d \sin\omega T - \omega^{-2}(1-\cos\omega T), \tag{20}$$

where $\omega^2 = K$. The next step is getting approximations for ω and consequently K. Straightforward calculations from the condition $\widetilde{L}(T = \widetilde{T}_c) = 1$ (see (16)) give

$$\tan\frac{\omega\widetilde{T}_c}{2} = -\omega L_d, \tag{21}$$

$$\tan\left(\pi - \frac{\omega\widetilde{T}_c}{2}\right) = \omega L_d$$

or

$$\omega = \frac{2(\pi - \arctan\omega L_d)}{\widetilde{T}_c}, \tag{22}$$

where $\widetilde{\omega}$ is the solution of (22) and $\widetilde{T}_c$ is calculated from the equation (19). From here we get $\widetilde{K} = \widetilde{\omega}^2$. Because equation (22) can not be solved analytically, Theorem 1, presented below, shows how the asymptotic expansion of ω looks like.

It is worth underlining that this type of approximation of the planar spring-mass dynamics may serve as an analytical tool for application in robotics and further research on legged locomotion (cf. [13], [12], [25]).

In the second part of this section, we will examine the behavior of approximations of L and θ, given by formulas (20) and (18), respectively. We start with Theorem 1, which presents the asymptotic solution of the equation (22).

Theorem 1 *Let $\widetilde{\omega} = a_{-1}\alpha^{-1} + a_0 + a_1\alpha + O(\alpha^2)$ be the solution of (22). Then,*

$$a_{-1} = \frac{\pi\theta_d}{2}, \quad a_0 = \frac{2}{\pi L_d}, \quad a_1 = -\frac{a_0^2}{a_{-1}} - \frac{\pi^2}{12a_{-1}}. \tag{23}$$

Moreover,

$$K^* \approx \widetilde{K}^* := \left(\frac{\pi\theta_d}{2\alpha}\right)^2 = \left(\frac{\pi}{2\alpha}\left(V_X\cos\alpha - V_Y\sin\alpha\right)\right)^2, \tag{24}$$

where K^* is the solution to the Problem (15). □

Proof We begin by finding the asymptotic behaviour of $\widetilde{\omega}\widetilde{T}_c/2$. Using the formula

$$\log\left(\frac{\theta_d+\alpha}{\theta_d-\alpha}\right)=\sum_{n=1}^{\infty}\frac{2\alpha^{2n-1}}{(2n-1)\theta_d^{2n-1}}\quad\text{for}\quad|\alpha|<\theta_d,\tag{25}$$

that is the Taylor expansion of the function $\widetilde{T}_c$ around $\alpha=0$, we get

$$\frac{\widetilde{\omega}\widetilde{T}_c}{2}=\frac{a_{-1}}{\theta_d}+\frac{a_0}{\theta_d}\alpha+\frac{a_1+a_{-1}/(3\theta_d^2)}{\theta_d}\alpha^2+O(\alpha^3).\tag{26}$$

Considering the term $(\pi-\arctan\omega L_d)$, the Taylor expansion to the second order about $\alpha=0$ is given by

$$\pi-\arctan\omega L_d=\frac{\pi}{2}+\frac{1}{L_d a_{-1}}\alpha-\frac{a_0}{L_d a_{-1}^2}\alpha^2+O(\alpha^3).\tag{27}$$

Next, a comparison of the respective coefficients of α^n in (26) and (27) leads to the following system of equations and solutions

$$\frac{a_{-1}}{\theta_d}=\frac{\pi}{2}\implies a_{-1}=\frac{\pi\theta_d}{2},\tag{28}$$

$$\frac{a_0}{\theta_d}=\frac{1}{L_d a_{-1}}\implies a_0=\frac{\theta_d}{L_d a_{-1}}=\frac{2}{\pi L_d},\tag{29}$$

$$\begin{aligned}\frac{a_1+a_{-1}/(3\theta_d^2)}{\theta_d}=-\frac{a_0}{L_d a_{-1}^2}\implies a_1&=-\frac{\theta_d a_0}{L_d a_{-1}^2}-\frac{a_{-1}}{3\theta_d^2}\\&=-\frac{a_0^2}{a_{-1}}-\frac{\pi^2}{12a_{-1}}.\end{aligned}\tag{30}$$

Analogously, we can count the successive coefficients of expansion $\widetilde{\omega}$, but for the sufficiently small initial angle α, the leading order of $\widetilde{\omega}$ is only the first component.

The last part of the proof is to find an approximation to K^*. We have

$$\widetilde{\omega}\approx\frac{\pi\theta_d}{2\alpha}\quad\text{as}\quad\alpha\to 0^+.\tag{31}$$

Remembering that $\omega^2=K$ yields (24) and the proof is complete. ∎

Because in the expansion of $\widetilde{\omega}$ we finally take into account only the first component $a_{-1}\alpha^{-1}$ and eliminate higher-order terms, the approximation $\widetilde{K}^*$ will reach lower values than $\widetilde{K}$. How both K^* parameter approximations $\widetilde{K}$ and $\widetilde{K}^*$ work will be presented in Section 4.

The same approximation of K^* as (24) was obtained in [28] with a use of asymptotic analysis (see Theorem 3 of [28]). Moreover, if we go back to (14) and express θ_d in terms of the Froude numbers V_X and V_Y, we see that $\theta_d\approx V_X$ for sufficiently small α. Hence, (24) reduces to

$$V_X\ll\sqrt{K},\quad K\gg 1.\tag{32}$$

Since $V_Y \leq V_X$, it can be concluded from the above that

$$\frac{V_X^2}{\sqrt{K}} \ll V_Y \ll \sqrt{K}, \quad K \gg 1. \tag{33}$$

By inserting the approximation (24) into (33) we get

$$\frac{2V_X}{\pi}\alpha \ll V_Y \ll \frac{\pi V_X}{2\alpha}, \tag{34}$$

which is consistent with the small angle assumption.

The authors of [20] presented several approximations of K^*. It turned out that the relationship between K^* and V_X should be quadratic for slower velocity values, while linear for faster velocities. In both cases, the numerical results were reproduced by the proposed empirical formulas. On the other hand, the approximations (24) proposed in this paper provide a systematic explanation of the leading order behaviour of K^* for small values of α. This can also be considered as an approximation of the quadratic part of the dependence on V_X.

At the end of this section we will show the asymptotic behaviour of L and θ as $K \to \infty$, where L and θ are solutions of the system (11) with the initial conditions (12). To simplify matters we set

$$\epsilon = \frac{1}{\sqrt{K}} \tag{35}$$

and we need to consider an expansion as $\epsilon \to 0^+$. Observe (see (20)) that

$$L(T) \approx \widetilde{L}(T) := 1 - \epsilon L_d \sin(\epsilon^{-1}T) + O(\epsilon^2), \quad \text{where} \quad \epsilon \to 0^+. \tag{36}$$

On the other hand, now we use the expansion in the Taylor series of $\widetilde{\theta}(T)$ (see (18))

$$\theta_d \sinh T - \alpha \cosh T = -\alpha + \theta_d T + O(T^2), \tag{37}$$

where $T = \epsilon\tau$ and $\tau < \infty$. An application of (37) yields

$$\theta(T) \approx \widetilde{\theta}(T) := -\alpha + \epsilon\theta_d + O(\epsilon^2), \quad \text{where} \quad \epsilon \to 0^+. \tag{38}$$

Combining this with Theorem 1 and Corollary 1 from [28] concludes the following results.

Theorem 2 *Let $(L(T), \theta(T))$ be the solution of the system (11). Next, the presented below asymptotic behaviour holds*

$$|L(T) - \widetilde{L}(T)| = O(\epsilon^2), \quad |\theta(T) - \widetilde{\theta}(T)| = O(\epsilon^2), \quad \text{as} \quad \epsilon \to 0^+ \tag{39}$$

uniformly for $T \leq \mathcal{T} < \infty$, where $\widetilde{L}$ and $\widetilde{\theta}$ are defined in (20) and (18), respectively. □

In Section 4 we will illustrate our results with several numerical simulations.

4. Numerical methods The method that allows to find an approximation of dimensionless stiffness was proposed by McMahon and Cheng in [20]. Taking specific values for V_X, V_Y and α, as well as an initial choice for the parameter K, the equations (11) with the initial conditions (12) were integrated forward while the leg was compressed and re-extended until it returned to full extension ($L = 1$). If the final leg angle was greater than α, the procedure was repeated using a higher value for K, if the final angle was less than α, the next approximation for the stiffness was smaller. Therefore the Problem (15) of Section 2.2 can easily be solved numerically using the shooting method. In the first step we use a numerical solver based on the fourth order Runge-Kutta method to solve the initial value problem (11) and (12) with a given K. Next, we find the T^* point such that $\theta(T^*, K) = \alpha$. In turn, $L(T^*, K)$ is contrasted with 1 and following the difference K value is corrected using the secant method in relation to the next iteration. The loop is continued until the required accuracy is achieved.

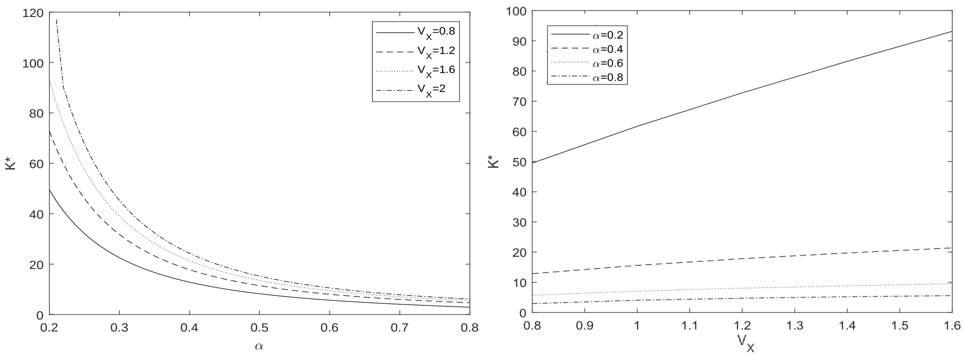

(a)

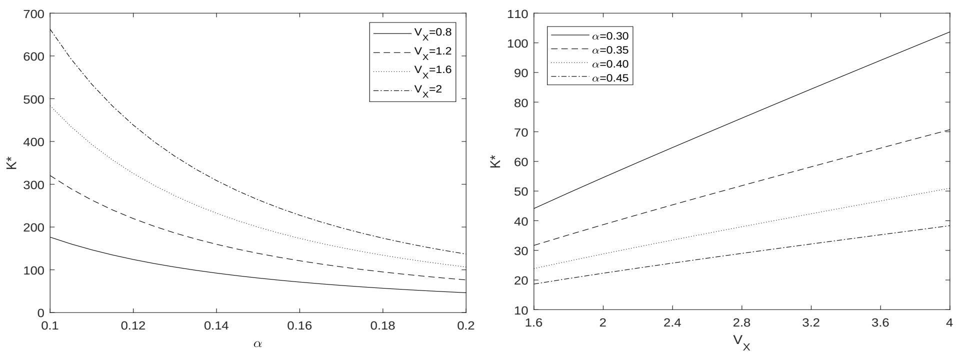

(b)

Figure 2: The numerical solution of Problem (15) from Section 2.2 for different sets of α and V_X with a fixed value of V_Y. (a) $V_Y = 0.1$ and (b) $V_Y = 0.2$.

Numerically found values of K^* are presented in Figure 2 in relation to the initial attack angle α for several V_X values and vice versa. Principally, not only for small angles, but also for the realistic regime of constants (see Table 1), we see that in general K^* is a moderately large parameter. The dependence on α and V_X is monotonic and we can predict that when V_X is the order of unity, K^* has a quadratic component of V_X (see (32)). In [28] these claims were proved along with showing existence and uniqueness for the main Problem from Section 2.2. Furthermore, as it is shown in part (b) on the right, K^* increases linearly with V_X in the range from $V_X = 1.6$ to 4. The linear behavior continues in the range above 4, although apparently this does not correspond to range used by "people and animals" from Table 1, and therefore does not appear in the plot. As shown, in parts (a) and (b) on the left, K^* increases rapidly when the initial leg angle decreases.

Finally, we present the results for a typical simulation of running (see [20]). The input parameters were chosen to represent a man of an average size: mass $= 72kg$, leg length$= 1.0m$, running at a moderate speed ($18.0km/h$, between 5 and 6 minutes per mile). Other parameters: $V_X = 1.60$, $V_Y = 0.245$ and $\alpha = 0.50$ (see Table 1 in [20]). The shooting method gives the following results

$$T^* = 0.622 \quad \text{and} \quad K^* = 15.493.$$

These parameters are obtained for a long-distance runner. As will be seen in Section 5, sprinters get a larger V_X parameter and a smaller α angle, and hence their K^* is more than four times bigger than the value presented above.

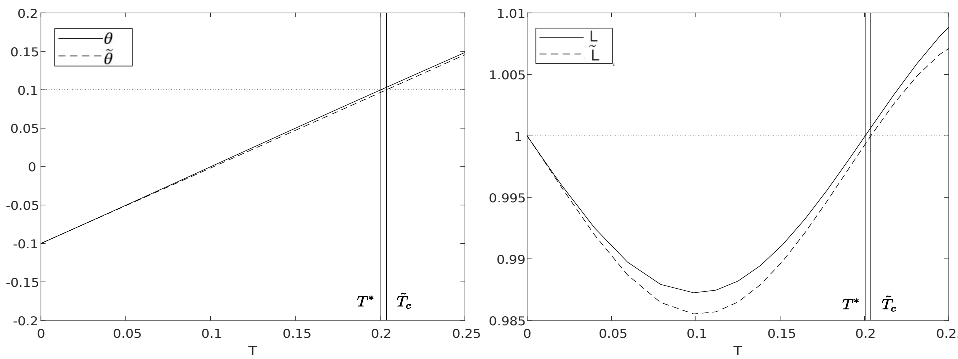

Figure 3: The comparisons between the numerically calculated values of θ and L, and their approximations $\widetilde{\theta}$ and $\widetilde{L}$, calculated from (18) and (20) for varying T. Solid vertical lines mark on the T-axis the values of T^* and $\widetilde{T}_c$. Here $\alpha = 0.1$, $V_X = 1$ and $V_Y = 0.1$.

At the end we will illustrate the results from Section 3 by using several numerical simulations. Therefore, at the beginning, we present comparisons between numerical values of θ and L, and their approximations $\widetilde{\theta}$ and $\widetilde{L}$, calculated from formulas (18) and (20), respectively. Figure 3 shows that both approximations work very well, implying that the difference between T^* (see Problem of Section 2.2) and $\widetilde{T}_c$ (cf. (19)) is negligible.

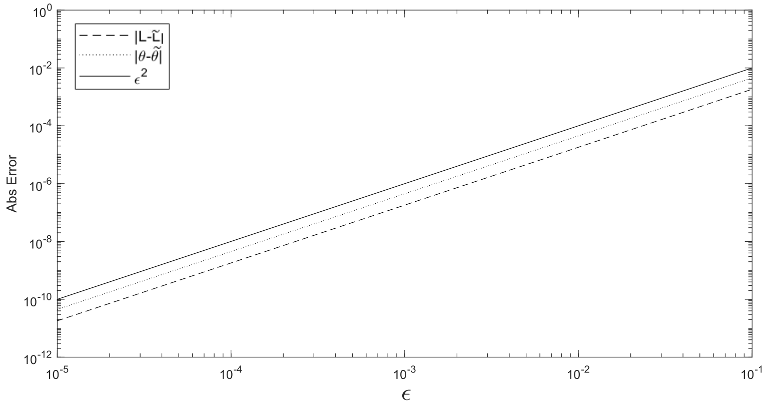

Figure 4: The absolute error of the approximations (18) and (20) of the solutions to (11) plotted on the log-log scale. The line $y = \epsilon^2$ is superimposed for the comparison. Here $\alpha = 0.1$, $V_X = 1$, $V_Y = 0.1$ and $T \in [0, \epsilon\pi]$.

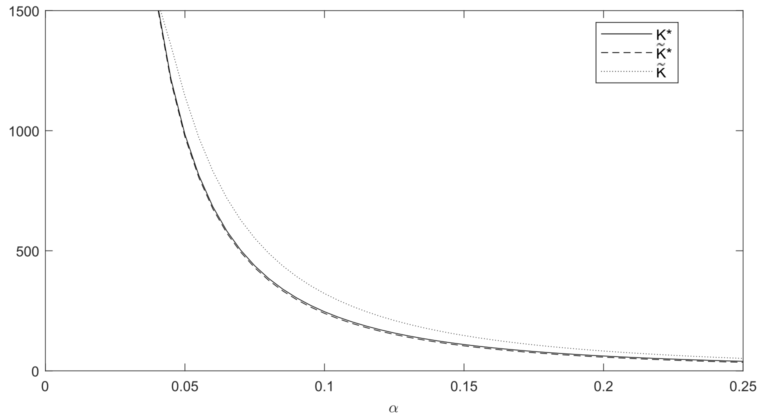

Figure 5: The comparison between the numerically calculated value of K^* and its approximations: $\widetilde{K}$ calculated from (22) and $\widetilde{K}^*$ calculated from (24) for varying α. Here $V_X = 1$ and $V_Y = 0.1$.

Moreover, on Figure 4 above, we can see an exemplary verification of Theorem 2. On the slow T scale (see [28]), at a compact interval $[0, \epsilon\pi]$ for the worst case $T = \epsilon\pi$, we calculated the error, i.e. the maximum difference of the solution of (11) with their approximations (18) and (20). On the log - log scale, the superimposed line $y = \epsilon^2$ indicates the correct order of convergence. Plots of the absolute errors for θ and L are parallel to this line. Also, notice that the original variables α, V_X and V_Y have been used.

The last example refers to the validity of $\widetilde{K}$ calculated from (22) as the approximation to the solution of the Problem from Section 2.2, that is K^*. As previously mentioned, the natural assumption for its accuracy is $\alpha \ll 1$, so we compare K^* with $\widetilde{K}$ for different values of the angle. Results are presented in Figure 5. We can see that along with the decrease of α both values are approaching each other, however, very slowly. In Figure 5, we can also see

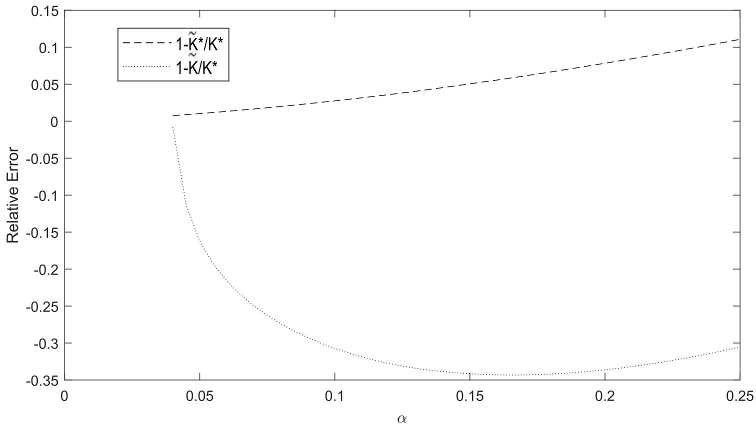

Figure 6: The relative error of the approximations $\widetilde{K}^*$ calculated from (24) and $\widetilde{K}$ calculated from (22) of K^* for varying α. Here $V_X = 1$ and $V_Y = 0.1$.

how the approximation $\widetilde{K}^*$ from Theorem 1 looks like. As we noted above, the approximation $\widetilde{K}^*$ given in (24) is the asymptotic leading order of the stiffness K^* (see [28]) and it agrees with $\widetilde{K}$ for $\alpha \to 0^+$. On the other hand, the approximation $\widetilde{K}$ was found by a heuristic, yet sensible, reasoning during which we may have lost some of the relevant information about the solution. Therefore, systematically derived $\widetilde{K}^*$ seems to be a better approximation of the stiffness for a decent range of α.

Figure 6 illustrates the relative errors of both approximations $\widetilde{K}^*$ and $\widetilde{K}$ in relation to K^* for varying α. Indeed, the approximation $\widetilde{K}^*$ behaves much better than $\widetilde{K}$. It turns out that $\widetilde{K}$ significantly overestimates the numerically calculated values, while $\widetilde{K}^*$ works almost perfectly in a certain α range.

5. Experiment and real data analysis In this section, the considered running model will be compared and verified with real data. The test material was collected from videos of athletes running short ($60m$) and long ($5000m$) distances. Four males and four females took part in the experiment. Half of them are sprinters and the rest are long - distance runners. Competitors with different physical parameters were selected. The camera was placed perpendicularly to the direction of the run. The optical axis of the camera has been aligned and the recording covers 10 meters. This allowed the athletes to demonstrate their usual running techniques without changing them in order to meet the requirements of the experiment (see [26]).

60: After a standard warm-up, each athlete performed one trial of a 60 - meter run. The run was interesting for us from the moment the sprinter reached submaximal velocity. The distance between 40 and 50 meters has been recorded. The athlete is then in the second of three phases of sprint running, so after the acceleration phase. At this moment the runner's body is straightened, and the step is full (see [8]).

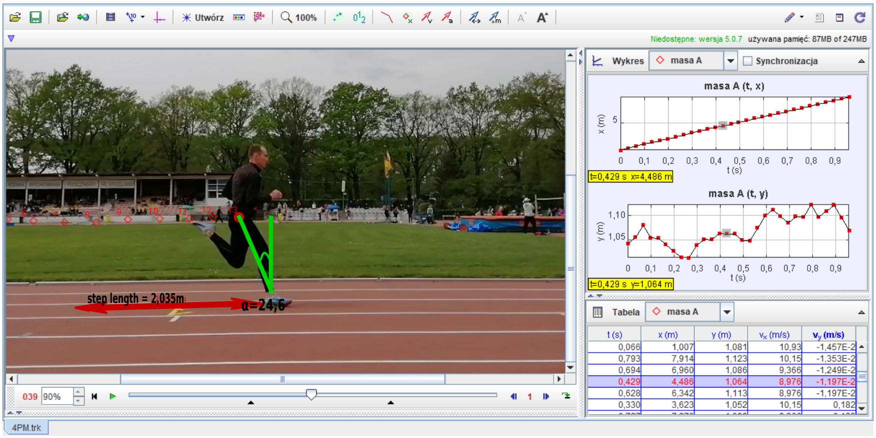

Figure 7: Tracker video analysis of the tested sprinter 4PM.

5000: The 5000 meters is a long - distance track event, where 12.5 laps are completed around the 400m track. In the competition (19. Memorial of Edward Listos, 29.05.2019 Wrocław), 10 meters in the straight line was recorded during the middle (sixth) lap.

The tracker Video Analysis for run modeling was used (see [5]). The video was divided into 0.033s frames. Which means that the trajectory of the point adopted as the center of mass (CoM) was followed with the frequency of 30Hz. Usually, a 10 meters long trail provides these people with 4 to 6 steps. The parameters in Tables 2, 3 and 4 are calculated as in Figure 7. In addition, $EX \pm SD$ is determined for each column of Tables 2, 3 and 4, which denotes the sample mean $\pm$ the sample standard deviation.

In the anatomical position, assuming the homogeneous gravitational field, the centre of mass (CoM) lies approximately anterior to the second sacral vertebra (see [15]). That is why the trajectory of the point is located at CoM level. So, the area of greater trochanter was studied (see [1]). In addition, l_0 is the relative length of the upper extremities from the greater trochanter area to the end of the heel bone. At the beginning, v_x and v_y were obtained. The average of the attack velocities of each step was calculated while running 10 meters. The values of l_0, v_x and v_y are presented in Table 2.

In our model, both the angle of attack and taking off are equal with accuracy to the mark (see BCs (16)). Real life is not as perfect as assumptions, so in the video analysis we observed that the taking off angle is usually greater than the attack angle. Therefore, α parameter was calculated by averaging the attack and taking off angles from the step, which was in front of the camera. It allows us to avoid errors resulting from a change of perspective. Interestingly, the difference in the attack angles for a group of sprinters is about 10° (0.17), while for long-distance runners the difference is bigger and is around 15° (0.26). This is due to the specifics of the step in the long-distance run, where

Athlete	Sex	Mass (kg)	l_0 (m)	v_x (m/s)	v_y (m/s)
			Sprint		
1EO	F	60	0.94	08.51	0.72
2AJ	F	57	0.99	10.53	0.69
3KA	M	74	1.00	09.65	0.64
4PM	M	76	1.08	09.54	0.67
EX		66.75	1.00	9.56	0.68
$\pm SD$		9.64	0.06	0.83	0.03
			Long-Distance		
5AM	F	51	0.85	4.41	0.81
6OW	F	48	0.96	4.23	0.85
7KK	M	69	1.15	5.82	0.80
8RM	M	68	1.10	5.69	0.78
EX		59	1.02	5.04	0.81
$\pm SD$		11.05	0.14	0.83	0.03

Table 2: Actual running parameters for the tested runners.

the back pendulum (during back swing, see [29]) dominates. Although the attack angle is much smaller during slow running [23], the average of angles causes in both groups the values of parameter α to be almost equal (see Table 3). However, it is important that measurements obtained from the video confirm correctness of the assumption about small α values in the model.

Additionally dimensionless parameters: V_X, V_Y appearing in the boundary conditions (12) can be found in Table 3. Horizontal and vertical Froude numbers (V_X, V_Y) were obtained from v_x and v_y by dividing them by reference velocity $(gl_0)^{1/2}$. Note that the dimensionless parameters of the tested runners are in typical ranges from Table 1.

The K^* and T^* parameters, presented in Table 4 below, have been numerically calculated. To describe the next parameter in Table 4, which is obtained from the model, let us recall the following relation

$$t_c^* = \sqrt{\frac{l_0}{g}} T^*, \tag{40}$$

where t_c^* is the contact time measured in seconds. Moreover, at this moment it is necessary to introduce a new symbol - swing time, denoted by t_s. It is time between two consecutive contacts of the same leg with the ground (i.e. $t_s = t_c + 2t_a$). In addition, Table 4 contains contact, aerial and swing times determined from the videos. Those parameters were computed by taking appropriate differences between the consecutive moments of taking off and landing. Moreover, note that the K^* parameter in the second group is clearly smaller (see Table 4). This fact is caused by about twice the value of the v_x parameter in the sprint group and a slight difference in α angles (see Tables 2 and 3).

Athlete	V_X	V_Y	α
	Sprint		
1EO	2.79	0.25	0.30
2AJ	3.39	0.23	0.37
3KA	3.08	0.21	0.33
4PM	2.93	0.22	0.32
EX	3.05	0.22	0.33
$\pm SD$	0.26	0.02	0.03
	Long-Distance		
5AM	1.41	0.25	0.26
6OW	1.35	0.27	0.24
7KK	1.73	0.24	0.27
8RM	1.74	0.24	0.28
EX	1.56	0.25	0.26
$\pm SD$	0.21	0.01	0.02

Table 3: Dimensionless parameters: V_X, V_Y and α for tested runners.

In addition, Table 4 also compares the length of the running step of a model and from the video. The length of the step, denoted by l_s, is obtained from the model using the formulas (4) and (5). So, we get that

$$l_s = 2l_0 \sin\alpha + v_x t_a, \tag{41}$$

where from (5) the aerial time is given by $t_a = \frac{2v_y}{g}$. Moreover, the step length from the video were computed using the ruler tool available in the Tracker program.

In order to verify the results from Table 4, a relative error was calculated for the parameters: t_c, t_a, t_s, l_s from the videos. Additionally, mean errors for the athletes of each class (sprinters and long-distance runners) were obtained as follows

$$\overline{\varepsilon}^j = \frac{1}{4}\sum_{i=1}^{4} \varepsilon_i^j, \tag{42}$$

where the relative error of the i-th athlete ($i = 1, 2, 3, 4$) from the j-class ($j = 1, 2$) is given by the formula

$$\varepsilon_i^j = \left| \frac{model_{value} - video_{value}}{video_{value}} \right|.$$

It is clearly visible that t_c is much better modeled for sprinters, while t_a for long-distance runners. In the final result, we have greater accuracy in modeling the running step for the second group.

6. Conclusions Modeling the contact phase is much more difficult than the aerial phase. We solved a nonlinear boundary value problem for the contact phase numerically. Moreover, after a justified simplification, we proposed

	From Model						From Video			
Athlete	K^*	T^*	t_c^* (s)	t_a (s)	t_s (s)	l_s (m)	t_c (s)	t_a (s)	t_s (s)	l_s (m)
	Sprint						Sprint			
1EO	81.579	0.214	0.067	0.154	0.375	1.87	0.074	0.156	0.396	1.86
2AJ	65.225	0.205	0.064	0.141	0.346	2.13	0.066	0.154	0.379	2.12
3KA	66.063	0.216	0.067	0.130	0.327	1.90	0.072	0.143	0.347	1.90
4PM	69.574	0.216	0.072	0.136	0.344	2.04	0.086	0.149	0.396	2.01
EX	70.610	0.213	0.068	0.140	0.348	1.99	0.075	0.151	0.380	1.97
$\pm SD$	7.551	0.005	0.003	0.010	0.020	0.122	0.008	0.006	0.023	0.117
	Long-Distance						Long-Distance			
5AM	54.186	0.373	0.110	0.165	0.440	1.16	0.127	0.174	0.475	1.16
6OW	61.723	0.358	0.112	0.167	0.446	1.19	0.121	0.176	0.483	1.19
7KK	52.407	0.341	0.117	0.165	0.447	1.57	0.151	0.166	0.483	1.57
8RM	57.044	0.351	0.117	0.159	0.443	1.50	0.156	0.160	0.476	1.49
EX	56.340	0.362	0.144	0.164	0.444	1.36	0.139	0.169	0.479	1.35
$\pm SD$	4.065	0.021	0.004	0.003	0.211	0.003	0.002	0.007	0.004	0.207

Table 4: The comparison of the contact time, the aerial time and the length of the running step from the model and from the video.

error	t_c	t_a	t_s	l_s
	Sprint			
ε_1^1	0.0946	0.0128	0.0285	0.0053
ε_2^1	0.0303	0.0844	0.0749	0.0047
ε_3^1	0.0694	0.0909	0.0866	0.0002
ε_4^1	0.1638	0.0872	0.1042	0.0015
$\overline{\varepsilon}^1$	0.0895	0.0668	0.0736	0.0029
	Long-Distance			
ε_5^2	0.1339	0.0517	0.0736	0.0025
ε_6^2	0.0744	0.0511	0.0571	0.0001
ε_7^2	0.2252	0.0060	0.0745	0.0019
ε_1^2	0.2500	0.0063	0.0861	0.0045
$\overline{\varepsilon}^2$	0.1708	0.0415	0.0918	0.0022

Table 5: Relative errors and mean relative errors of parameters t_c, t_a, t_s, l_s.

an approximate solution to this problem. It turned out that the approximation of K^* presented in Theorem 1 is correct, especially for small values of α. K^* is directly proportional to V_X^2 and inversely proportional to α^2. Additionally, as it can be seen from the results in Theorem 2, the asymptotic solutions of the nonlinear equations work very well as $K \to \infty$.

During the experiment we observed that a faster run can generate a greater attack angle. The model works better for smaller α, so it is not surprising that the general accuracy obtained in the long - distance running was slightly better. It is worth noting, however, that in both groups the measurements confirm the smallness of angle α, which is also the parameter that has the most affect on K^*. Also, increasing the Froude numbers V_X and V_Y indicate higher values of K^*, but the scale of changes is incomparably small.

In the high - speed running, the disproportion of t_a and t_c was observed: i.e. $t_c < t_a$. This results from the fact that the average vertical force during the contact time is usually greater than mg, whereas during the aerial time, it cannot be exceeded. In the long - distance running, the aerial time is similar to the contact time $t_a \sim t_c$ (see [6]). The ranges and dependence between these parameters are closely related to the specifics of the two types of running considered in the paper (see [24], [23]). The aerial time t_a is mostly dependent on v_y, but also on α, while the contact time t_c is mostly associated with α (CoM need to overcome a longer way) and less with v_x (velocity of overcoming this way). We obtained more accurate results for t_a, because the driving forces are more predictable and we have the direct solution.

Even though all the parameters are in the typical ranges, it is necessary to remember that these are dependent on the individual traits of the athlete. That is why there are some errors of the parameter predictions from the model when compared to the video analysis. However, the smallest mean relative error is for the step length, because partial inaccuracies eliminate each other during the calculations. This indicates a good holistic operation and application of the model.

The results of the experiment show that moving away from symmetry in boundary conditions will bring the model closer to a real running step. Therefore, using the considerations of Geyer et al. [13], further work will consist of examining the stability of the approximate solution for the dynamics of the planar spring-mass model. In our study, the scope of stability in the spring-mass running will be investigated by comparing a return-map analysis based on the approximation with numerical results throughout the range of the parameters: the spring stiffness and the angle of attack. We intend to periodically attach the aerial phase of the movement, then determine the initial angle related to the state at the touch-down and the take-off angle from the condition for attaining the equilibrium length of the spring and also check how the spring amplitude of deflections behaves in each subsequent contact phase. On the other hand, we will use the fact that our approximate solution has been systematically derived from the singular perturbation theory (cf. [28]).

References

[1] M. Adolphe, J. Clerval, Z. Kirchof, R. Lacombe-Delpech, and B. Zagrodny. Center of mass of human's body segments. *Mechanics and Mechanical Engineering*, 21(3):485–497, 2017. URL http://kdm.p.lodz.pl/articles/2017/3/21_3_4.pdf. Cited on p. 40.

[2] R. M. Alexander. Energy-saving mechanisms in walking and running.

Journal of Experimental Biology, 160(1):55–69, 1991. URL http://e.guigon.free.fr/rsc/article/AlexanderRM91.pdf. Cited on p. 25.

[3] T. Anderson. Biomechanics and running economy. *Sports Medicine*, 22 (2):76–89, 1996. doi: 10.1007/s40279-016-0474-4. Cited on p. 25.

[4] R. Blickhan. The spring-mass model for running and hopping. *Journal of Biomechanics*, 22(11/12):1217–1227, 1989. doi: 10.1016/0021-9290(89)90224-8. Cited on pp. 26 and 27.References

[5] D. Brown. Tracker Video Analysis, 2013. Tracker is a free video analysis and modeling tool built on the Open Source Physics (OSP) Java framework. It is designed to be used in physics education. Tracker video modeling is a powerful way to combine videos with computer modeling. For more information see Particle Model Help or AAPT Summer Meeting posters Video Modeling (2008) and Video Modeling with Tracker (2009). Tracker Video Analysis https://www.physlets.org/tracker/. swZbl 27291. Cited on p. 40.

[6] G. A. Cavagna, P. Franzetti, N. C. Heglund, and P. Willems. The determinants of the step frequency in running, trotting and hopping in man and other vertebrates. *Journal of Physiology*, 399:89–92, 1988. doi: 10.1113/jphysiol.1988.sp017069. PubMed Central PMCID: PMC1191653 . Cited on p. 44.

[7] S. Collins, A. Ruina, R. Tedrake, and M. Wisse. Efficient bipedal robots based on passive-dynamic walkers. *Science*, 307(5712):1082–1085, 2005. doi: 10.1126/science.1107799. Cited on p. 26.

[8] C. Cronin and K. T. Hansen. Resisted sprint training for the acceleration phase of sprinting. *Strength and Conditioning Journal*, 28(4):42–53, 2006. doi: 10.1519/00126548-200608000-00006. Cited on p. 39.

[9] J. T. Daniels, R. A. Yarbrough, and C. Foster. Changes in $\dot{V}O_2$ max and running performance with training. *European Journal of Applied Physiology and Occupational Physiology*, 39(4):249–254, 1978. doi: 10.1007/bf00421448. Cited on p. 25.

[10] M. H. Dickinson, C. T. Farley, R. J. Full, M. A. R. Koehl, R. Kram, and S. Lehman. How animals move: an integrative view. *Science*, 288(5463): 100–106, 2000. doi: 10.1126/science.288.5463.100. Cited on p. 25.

[11] C. T. Farley, J. Glasheen, and T. A. McMahon. Running springs: speed and animal size. *Journal of Experimental Biology*, 185:71–86, 1993. URL https://pdfs.semanticscholar.org/813d/6358ca53e019bec3e60db9ae6d0fda4b71d4.pdf. Cited on p. 31.

[12] H. Geyer and U. Saranli. Gait based on the spring-loaded inverted pendulum. In A. Goswami and P. Vadakkepat, editors, *Humanoid Robotics: A Reference*, pages 923–947. Springer, Dordrecht, 2017. doi: 10.1007/978-94-007-6046-2. Cited on p. 33.

[13] H. Geyer, A. Seyfarth, and R. Blickhan. Spring-mass running: simple

approximate solution and application to gait stability. *J. Theoret. Biol.*, 232(3):315–328, 2005. ISSN 0022-5193. doi: 10.1016/j.jtbi.2004.08.015. MR 2120902; PMID: 15572057 . Cited on pp. 32, 33, and 44.References

[14] H. Geyer, A. Seyfarth, and R. Blickhan. Compliant leg behaviour explains basic dynamics of walking and running. *Proc.of the Royal Society B: Biol. Sci.*, 273(1603):2861–2867, 2006. doi: 10.1098/rspb.2006.3637. PubMed Central PMCID: PMC1664632 . Cited on p. 26.

[15] S. J. Hall. Equilibrium and human movement. In *Basic Biomechanics*, pages 433–435. McGraw–Hill, 2015. Online available at www.ftramonmartins.files.wordpress.com. Cited on p. 40.

[16] A. Heck and P. Uylings. A jump forwards with mathematics and physics. In M. Joubert, A. Clark-Wilson, and M. McCabe, editors, *Enhancing Mathematics Education Through Technology, Proceedings of ICTMT10*, pages 129–134. Portsmouth, UK: University of Portsmouth, 2011. doi: 11245/1.360153. Online available at https://pdfs.semanticscholar.org. Cited on p. 27.

[17] P. Holmes, R. J. Full, D. Koditschek, and J. Guckenheimer. The dynamics of legged locomotion: models, analyses, and challenges. *SIAM Rev.*, 48(2):207–304, 2006. ISSN 0036-1445. doi: 10.1137/S0036144504445133. MR 2240592. Cited on p. 26.

[18] Ł. Kidziński, S. P. Mohanty, C. Ong, Z. Huang, S. Zhou, A. Pechenko, A. Stelmaszczyk, P. Jarosik, M. Pavlov, S. Kolesnikov, S. Plis, Z. Chen, Z. Zhang, J. Chen, J. Shi, Z. Zheng, C. Yuan, Z. Lin, H. Michalewski, P. Miłoś, B. Osiński, A. Melnik, M. Schilling, H. Ritter, S. Carroll, J. Hicks, S. Levine, M. Salathé, and S. Delp. Learning to Run challenge solutions: Adapting reinforcement learning methods for neuromusculoskeletal environments. In *The NIPS'17 Competition: Building Intelligent Systems*, pages 121–153. Springer, Cham, 2018. Online available at arXiv:1804.00361. Cited on p. 26.

[19] P. Maquet. Borelli: De motu animalium. A first treatise on biomechanics. *Acta Orthopaedica Belgica*, 55(4):541–546, 1989. Cited on p. 26.

[20] T. A. McMahon and G. C. Cheng. The mechanics of running: How does stiffness couple with speed? *Journal of Biomechanic*, 23(1):65–78, 1990. doi: 10.1016/0021-9290(90)90042-2. Cited on pp. 26, 27, 29, 31, 35, 36, and 37.References

[21] A. Merker, D. Kaiser, and M. Hermann. Numerical bifurcation analysis of the bipedal spring-mass model. *Phys. D*, 291:21–30, 2015. ISSN 0167-2789. doi: 10.1016/j.physd.2014.09.010. URL `https://doi.org/10.1016/j.physd.2014.09.010`. Cited on p. 26.

[22] S. Mochon and T. A. McMahon. Ballistic walking. *Journal of Biomechanics*, 13(1):49–57, 1980. doi: 10.1016/0021-9290(80)90007-x. Cited on p. 26.

[23] J. B. Morin, K. Tomazin, P. Edouard, and G. Y. Millet. Changes in running mechanics and spring - mass behavior induced by a mountain ultra-marathon race. *Journal of Biomechanics*, 44(6):1104–1107, 2011. doi: 10.1016/j.jbiomech.2011.01.028. Cited on pp. 41 and 44.References

[24] J. B. Morin, M. Bourdin, P. Edouard, N. Peyrot, P. Samozino, and J. R. Lacour. Mechanical determinants of 100-m sprint running performance. *European Journal of Applied Physiology*, 112(11):3921–3930, 2012. doi: 10.1007/s00421-012-2379-8. Cited on p. 44.

[25] R. Müller, A. V. Birn-Jeffery, and Y. Blum. Human and avian running on uneven ground: a model-based comparison. *Journal of the Royal Society Interface*, 13(122):1–8, 2016. doi: 10.1098/rsif.2016.0529. PubMed Central PMCID: PMC5046951 . Cited on p. 33.

[26] O. Nemtsev, N. Nemtseva, and J. Kucherenko. Comparison of technique characteristics of sprint running at maximal and submaximal speeds. In *33d International Conference on Biomechanics in Sports*. Poitiers, France, 2015. URL `https://isbs2015.sciencesconf.org/57286/document`. Cited on p. 39.

[27] M. C. Nussbaum. *Aristotle's De Motu Animalium: Text with translation, commentary, and interpretive essays*. Princeton University Press, 1985. ISBN 9780691020358. Asturias Award for Social Sciences. Cited on p. 26.

[28] Ł. Płociniczak and Z. Wróblewska. Solution and asymptotic analysis of a boundary value problem in the spring-mass model of running. *To appear in Nonlinear Dynamics, arXiv:1903.02247*, 2019. doi: 10.1007/s11071-019-05462-z. Cited on pp. 26, 34, 35, 37, 38, 39, and 44.References

[29] J. Puleo and P. Milroy. *Running Anatomy*. Human Kinetics Australia, Champaign, IL, United States, first edition, 2010. ISBN 1492548294. Cited on p. 41.

[30] U. Saranli and D. E. Koditschek. Template based control of hexapedal running. In *Proceedings of the IEEE International Conference on Robotics and Automation*, pages 1374—-1379. Taipei, Taiwan, 2003. doi: 10.1109/ROBOT.2003.1241783. Cited on p. 26.

[31] S. Siegler, R. Seliktar, and W. Hyman. Simulation of human gait with the aid of a simple mechanical model. *Journal of Biomechanics*, 15(6): 415–425, 1982. doi: 10.1016/0021-9290(82)90078-1. Cited on p. 26.

[32] M. Srinivasan and P. Holmes. How well can spring-mass-like telescoping leg models fit multi-pedal sagittal-plane locomotion data? *Journal of Theoretical Biology*, 255(1):1–7, 2008. doi: 10.1016/j.jtbi.2008.06.034. Cited on p. 26.

[33] K. R. Williams and P. R. Cavanagh. Relationship between distance running mechanics, running economy, and performance. *Journal of Applied Physiology*, 63(3):1236–1245, 1987. doi: 10.1152/jappl.1987.63.3.1236.

Cited on p. 25.

Przybliżone rozwiązania i analiza numeryczna modelu masy sprężynowej dla biegania

Zofia Wróblewska

Streszczenie W pracy rozważamy klasyczny model masy sprężynowej dla biegania oparty na odwróconym elastycznym wahadle. Przedstawiamy nowe przybliżone rozwiązanie interesującego zagadnienia brzegowego dla układu dwóch nieliniowych równań różniczkowych, które w naturalny sposób uzyskujemy w tym modelu. Badamy asymptotyczne zachowanie uzyskanych aproksymacji i podajemy asymptotyczną postać współczynnika spężystości nogi dla małych kątów ataku. Symulacje pokazują, że nowe rozwiązanie wypadło bardzo dobrze i wykazało dużą zgodność przybliżenia z rozwiązaniem dokładnym. Nasze wyniki zostały zilustrowane kilkoma praktycznymi przykładami pokazując, że pomiary parametrów biegu lekkoatletów są bliskie wartościom uzyskanym z modelu.

Klasyfikacja tematyczna AMS (2010): 34E05; 34B15.

Słowa kluczowe: model masy srężynowej, krok biegowy, wahadło sprężynowe, zagadnienie brzegowe, rozwiązanie przybliżone, metoda strzelania.

Zofia Wróblewska received BSc degree in Applied Mathematics in 2018, and in 2019 she have gotten a master's degree in Applied Mathematics at Wrocław University of Science and Technology, Poland. Her specialty is Mathematics for Industry and Commerce. During her studies she had a one semester exchange in Portugal at Técnico Lisboa as an Erasmus student. The reason she chose this direction, as she often mentions, is interest in mathematics, the ability to model the surrounding reality and to study it with the help of created models. Particularly interested in biology and mechanisms allowing the movement of living beings, including man. The issues related to the mechanisms of movement of the human body were tested in practice. After graduating, feeling the need to deepen knowledge of her interests, she began research in biomechanics as part of the doctoral school at the Wrocław University of Science and Technology and studies at the University School of Physical Education in Wrocław, where she specializes in issues related to training athletes.

Zofia Wróblewska
Wrocław University of Science and Technology
Faculty of Pure and Applied Mathematics
Wybrzeże Wyspiańskiego 27, 50-370 Wrocław, Poland
E-mail: `Zofia.Wroblewska@pwr.edu.pl`

Communicated by: Wojciech Mitkowski

(Received: 31th of July 2019; revised: 21th of January 2020)